https://doi.org/10.1038/s44328-024-00012-z

Label-free functional imaging of vagus nerve stimulation-evoked potentials at the cortical surface

Laura RoaFiore[1,3] ✉, Trevor Meyer[1,3], Thaissa Peixoto[1] & Pedro Irazoqui[1,2]

Vagus nerve stimulation (VNS) is an FDA-approved stimulation therapy to treat patients with refractory epilepsy. In this work, we use a coherent holographic imaging system to characterize vagus nerve-evoked potentials (VEPs) in the cortex in response to VNS stimulation paradigms without electrode placement or any genetic, structural, or functional labels. We analyze stimulation amplitude up to saturation, pulse width up to 800 μs, and frequency from 10 Hz to 30 Hz, finding that stimulation amplitude strongly modulates VEPs response magnitude (effect size 0.401), while pulse width has a moderate modulatory effect (effect size 0.127) and frequency has almost no modulatory effect (effect size 0.009) on the evoked potential magnitude. We find mild interactions between pulse width and frequency. This non-contact label-free functional imaging technique may serve as a non-invasive rapid-feedback tool to characterize VEPs and may increase the efficacy of VNS in patients with refractory epilepsy.

Epilepsy is a neurological disorder characterized by predisposition for unprovoked seizures with a high risk of recurrence. Its prevalence and burden are relatively high, with 7.60 per every 1000 people affected over a lifetime[1,2]. While a portion of patients with epilepsy may become seizure-free through treatment with anti-epileptic drugs (AEDs), 2040% of patients will continue to have seizures[3]. These patients have "refractory" epilepsy, and treatment options range from surgical resection of epileptogenic zones to implantation of surgical stimulation devices.

One treatment falling within the latter category is vagus nerve stimulation (VNS). VNS has been an FDA-approved treatment for medically refractory epilepsy for over two decades, and its use has lately expanded to medication-resistant depression, inflammation control, metabolic syndrome, and rehabilitation aid for stroke[4]. This treatment involves the surgical implantation of a pulse generator near the patient's clavicle and electrical leads that terminate in electrodes wrapped around the vagus nerve. The system delivers electrical impulses to the vagus nerve at programmed intervals to modulate the activity of the nerve. There are many adjustable stimulation parameters defining the applied stimulation for each patient—including amplitude, pulse width, and frequency—which must be decided and fine-tuned individually after implantation.

Original parameters for clinically implanted VNS devices came from a study conducted on dogs in 1992[5]. These parameters were later employed in the initial clinical trials for VNS in epileptic patients and later on in patients with depression[6–8]. It was later suggested that modifying these stimulation parameters could optimize the efficacy outcomes of treatment in refractory patients[9]; however, population studies across animals, as well as clinical studies examining this theory, were widely variable in result, making it difficult to compare and contrast parameter optimization. Additionally, some of these studies reached contradictory conclusions on effective parameter combinations—further confounding the process of parameter selection[10,11]. The dilemma facing these studies was largely the same and arose primarily due to the difficulty in obtaining feedback on the efficacy of chosen parameters. As the clinical endpoint for VNS parameter selection is a reduction in seizure frequency, determining success requires weeks to months of waiting to determine the rate of spontaneous seizure occurrence—a process that is plagued by many confounding variables that simultaneously impact seizure onset.

Unfortunately, as these previous studies underscore, optimizing stimulation parameters for individual patients remains a tedious process without any rapid-feedback tools like functional imaging protocols to improve efficacy. Manufacturer guidance suggests that clinicians begin with the most efficacious settings for their device and electrode, and make incremental changes based on observed seizure-reduction in the weeks to months after each change[12]. Some studies have also used pain and perception thresholds as reference points for calibration, or other peripheral mechanisms like heart rate and heart rate variability[4,11,12]. The starting value for stimulation intensity (current amplitude) is 0.25 mA in nearly all patients. Depending on the patient's responsiveness to this initial intensity,

[1]Department of Electrical and Computer Engineering, The Johns Hopkins University, Baltimore, MD, USA. [2]Department of Biomedical Engineering, The Johns Hopkins University, Baltimore, MD, USA. [3]These authors contributed equally: Laura RoaFiore, Trevor Meyer. ✉e-mail: lroa2@jhu.edu

stimulation is then increased to a range of 1.25—2.00 mA over the next few months. The most prevalent stimulation settings outside of the intensity are pulse width 250—500 μs, frequency (20–30 Hz), and time cycling (30 s on and 3–5 minutes off).

Prior investigations into central nervous system responses to VNS involve the use of methodologies such as functional magnetic resonance imaging (fMRI) as well as electroencephalography (EEG). However, these studies have often produced conflicting results even on the functional response to stimulation. Recent work using EEG has found that VNS stimulation at 10 Hz can produce changes to EEG power[13,14]; however, these results directly contradict findings from prior EEG studies, which found that stimulation frequencies did not produce any observable effects on EEG power[15,16]. Recent fMRI findings showed distinct differences in effects between invasive VNS and transcutaneous VNS[17]. Additionally, invasive EEG studies on acute invasive VNS have found opposing effects of similar stimulation parameters on EEG spectral and broadband power[18,19]. A more recent finding suggests that while there may be variable results across cortical networks in the stereotactic EEG of different patients, in some individuals, there are distinctly similar responses with certain stimulation paradigms[13]. A possible explanation for the high variability in functional imaging results across the prior literature lies in EEG and fMRI's lack of highenough spatiotemporal resolution to capture the subtle effects of VNS on cortical circuits.

Several problems thus remain with VNS: namely, there is no label-free modality with a high enough spatiotemporal resolution to visualize a patient's VNS-evoked neural response in the cortex as required to tune their stimulus parameters for enhanced treatment efficacy. We utilize a coherent optical system to characterize the dynamics of vagus nerve-evoked potentials (VEPs) at the cortical surface. Visualization of the VEP modulation was then recorded as a function of the stimulation amplitude, pulse width, and frequency. We demonstrate that VEPs are strongly modulated by stimulation current amplitude and moderately modulated by stimulation pulse width, while there is little to no short-term modulation as a result of stimulation frequency. We find that an effect size analysis supports these conclusions, with stimulus amplitude having the largest effect size and stimulus frequency having the smallest.

Other technologies can extract similar in-vivo neural activation, including calcium imaging (GCaMP6), optogenetics, and electrical recordings using high-density grids and shanks, yet each brings limitations. GCaMP6 and optogenetics introduce extended experimental timelines to allow for viral or genetic adoptions of fluorescent tags, which can risk additional adverse events, complicate housing, add husbandry protocols, and put limitations on animal age. Also, fluorescent-based systems often image only a few cells, which does not capture bulk firing, or suffer from saturation when viewing large areas and networks during times of strong activation like we see in VEPs. Other drawbacks of more invasive techniques, like high-density electrode recordings, include the breaking of the dura and the insertion of foreign material, which risks disrupting or harming the delicate neural circuits of interest. Our label-free, non-contact techniques avoid each of these disruptions, supporting convenient, easy-to-use rapid-feedback imaging of the natural untouched neural tissue without the need for labels by merely observing reflected infrared light at skin-safe power levels. Holographic techniques also support high spatial resolution across a large field of view (FOV) that can capture the dynamics of entire cortical regions with great fidelity.

The use of coherent holographic imaging to visualize the dynamics and modulation of vagus-evoked potentials at the cortical surface explored in this study is a novel, promising step towards visualizing neural responses to VNS for the purpose of enabling objective, quantitative feedback of stimulation efficacy. This manuscript aims to demonstrate the validity of this functional imaging technique and to thoroughly characterize vagus-evoked responses as they relate to the following VNS stimulation parameters: amplitude, pulse width, and frequency. Success in quantifying VNS stimulation parameters in rodents will motivate future studies in translating this functional imaging technique to humans.

Results

Electrical validation

It was first necessary to validate the concordance of the recorded optical signal with a recorded electrical signal at the site of imaging. For this reason, a twisted pair electrode (see "Effect Size and Interaction") was used to record evoked electrical activity on an exposed section of the cortex during VNS stimulation. The optical signal was recorded concomitantly with the electrical signal during stimulation, and the signals were compared. The rising edge of the optical signal grew in tandem with the electrical signal (see Fig. 1B), confirming a correlating dose-dependent response behavior in both the electrical and optical recordings. This protocol was confirmed in multiple animals ($N = 4$ animals), and shape-matching, dose-dependent responses were observed between both signals. While the shape of the signal following the initial stimulus-locked response sometimes varied, there was always a correlation between the shape and magnitude of the initial upward deflection in both signals. One notable observation from Fig. 1 is that the shape of the first minimum of the signal, which is sometimes double or single-peaked, consistently matches across trials and animals.

Amplitude characterization

The amplitude characterization test demonstrated a clear increase in the response magnitude as stimulation current amplitude increased (see Fig. 2A,

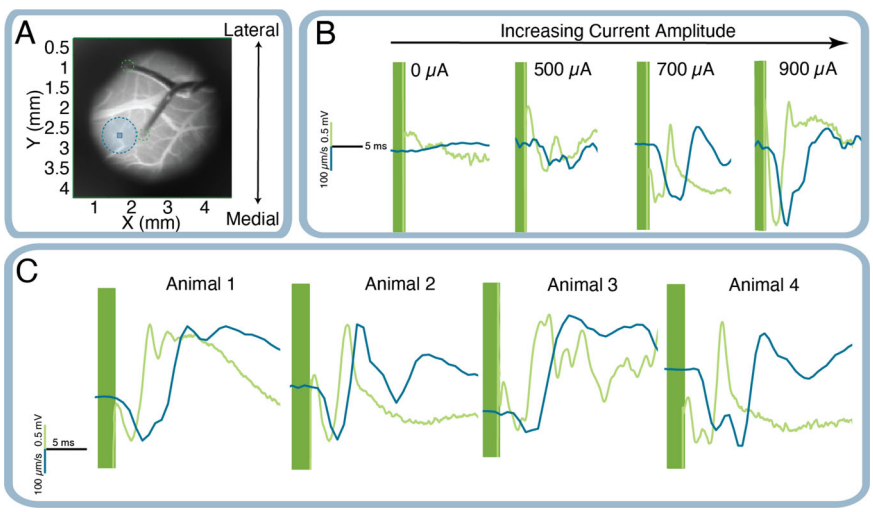

Fig. 1 | Comparison of the electrical signal (green) with the optical signal (blue). The stimulus artifact, present only in the electrical signal, was easily visually separated from the dose-dependent response and is redacted with green vertical bars to simplify interpretation. **A** Full FOV showing the cortex with a twisted pair electrode in view. The optical ROI was placed in between the electrode tips while avoiding large vasculature, and is outlined in a blue dotted circle. The electrode tips sourcing our differential recording are outlined in a green dotted circle. **B** Representative application of stimulus with no, low, medium, and high amplitude, respectively. **C** Representative examples of responses from four animals. Although animals often had different response shapes, the rising edge considered in this study was a consistently matching feature.

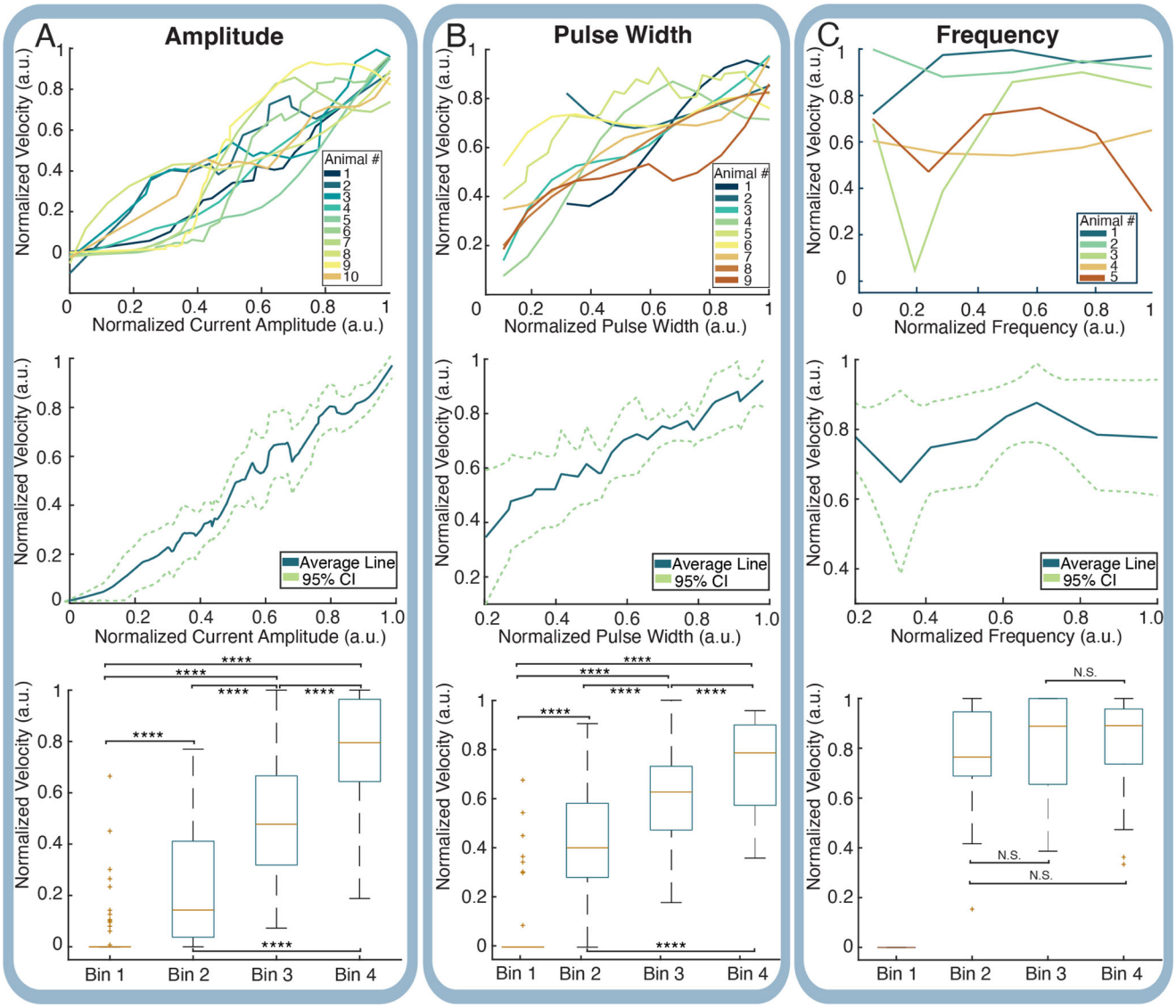

Fig. 2 | Analysis of response curves considering response magnitude related to stimulus amplitude, pulse width, and frequency. Statistical significance is indicated in relevant figures. ****$p < 1E\text{-}04$(A). VNS was performed using sets of randomized parameters (amplitude, pulse width, frequency), holding other parameters constant. As amplitude values increased, the neural response recorded optically also increased correspondingly. Pulse width demonstrated a similar relationship. Increases in frequency were not observed to have a strong relationship to neural responses. **A** Top—Amplitude response curves from all animals. Center—average amplitude response curve, with a 95% confidence interval. Bottom—Comparison of response magnitude from stimulus amplitude quartiles. **B** Top—Pulse Width response curves from all animals. Center—average pulse width response curve, with a 95% confidence interval. Bottom—comparison of response magnitude from stimulus pulse width quartiles. **C** Top—frequency response curves from all animals. Center—average frequency response curve, with a 95% confidence interval. Bottom—comparison of response magnitude from stimulus frequency quartiles.

top panel), both within and across animals ($N = 10$ animals, 30 trials). When averaged across all trials across all animals, the resultant average input–output response to current amplitude was exponential in nature (see Fig. 2A, middle panel), as is expected from neural input–output curves in prior literature[20,21]. To perform significance tests, normalized neural responses were placed into quartile bins according to the normalized amplitude tested. These bins were as follows: 0–0.25, 0.25–0.5, 0.5–0.75, and 0.75–1.0 of the maximum amplitude tested, and significance between each bin was tested with Welch's t test (see "Statistical analyses" for statistical methodology). There was a high level of significance between the neural responses categorized in all quartiles. P values between each quartile were extremely significant (see Fig. 2A, bottom panel). All of these response patterns remained consistent after the application of a paralytic and after the cessation of diaphragmatic deflection following euthanasia injection. Data for these trials can be found in the supplementary information (Supplementary Fig. 3). These paralyzed and post-mortem controls, along with the electrical validation results, support that the measured response originated from stimulus-triggered aggregate neural responses and was not driven by motion artifact or other physiological correlates.

Pulse width characterization

The pulse width characterization test also demonstrated an increase in the neural response signal magnitude as stimulation pulse width increased, although it was slightly less marked than that for amplitude (see Fig. 2B, top panel). This was observed both within and across animals ($N = 9$ animals, 27 trials). As with amplitude, when averaged across all trials across all animals, the resultant average input–output response to pulse width followed an upward trend (see Fig. 2B, middle panel). To perform significance tests across animals, normalized neural responses were placed into quartile bins according to the normalized pulse widths of 0–0.25, 0.25–0.5, 0.5–0.75 and 0.75–1.0 of the maximum pulse width tested. There was a high level of significance between the neural responses categorized in each quartile as

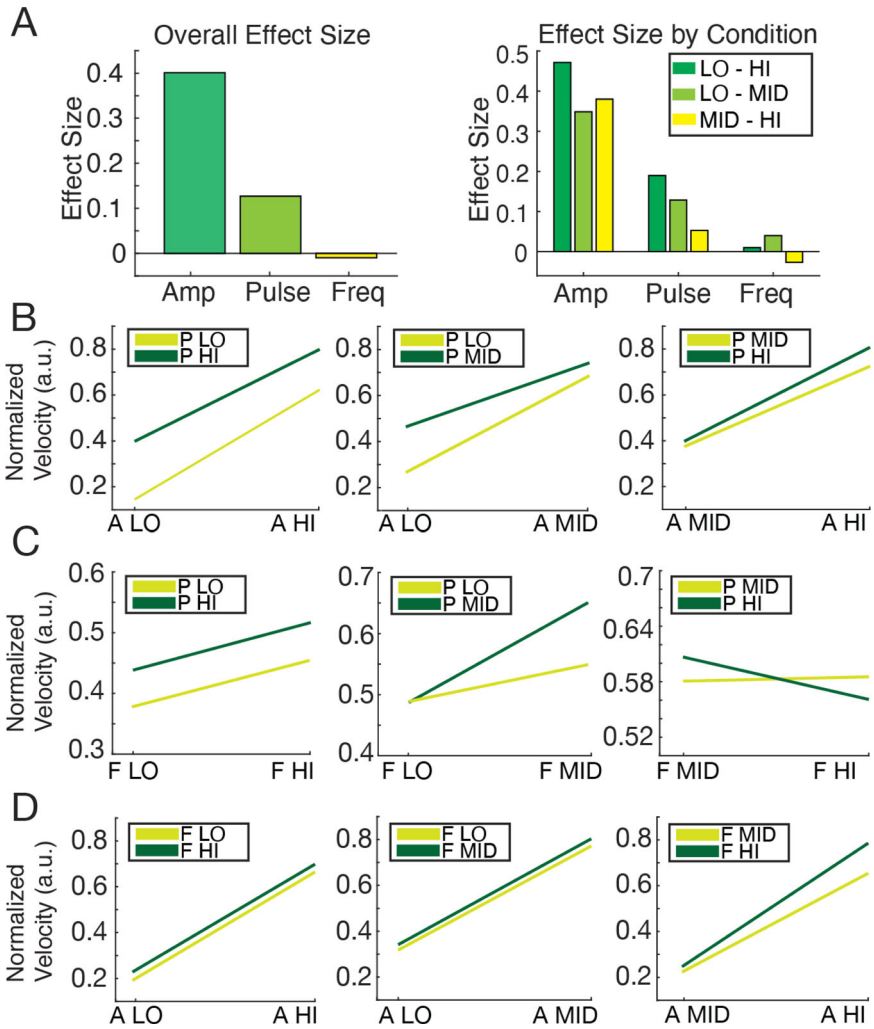

Fig. 3 | Analysis of Cohen's D values of effect size for VEP response related to amplitude (abbreviated "Amp" or "A"), pulse width (abbreviated "Pulse" or "P"), and frequency (abbreviated "Freq" or "F"). **A** Left—overall effect size for each parameter, showing amplitude with the greatest effect size ($d = 0.401$), pulse width with a moderate effect size (d=0.127), and frequency with the lowest (0.009). Right—effect size of each condition, illustrating which parameter magnitudes have the greatest effect. **B** Interaction plots for amplitude and pulse width. All plots have no intersecting points, indicating no interaction. **C** Interaction plots for frequency and pulse width. Pulse width and frequency have interactions, with P-MID and F-MID showing a larger response than P-HI F-HI and P-LO F-LO. **D** Interaction plots for amplitude and frequency. All plots have no intersecting points, indicating no interaction.

p values between all quartiles were at 1.19E-05 and lower. Just as with the amplitude characterization, these response patterns remained the same in paralyzed and post-mortem trials.

Frequency characterization

The frequency characterization test did not demonstrate as much of an effect on the neural response signal magnitude as frequency increased, either within animals or across animals ($N = 5$ animals, 15 trials) (see Fig. 2C, top panel). When averaged across animals and trials, the neural response to frequency was minimal (see Fig. 2C, middle panel), and while there was significance between the first quartile and all other quartiles (see Fig. 2C, bottom panel), Welch's t test revealed there was no significance between other quartile relationships.

Parameter effect size and interaction

Stimulation current amplitude had the largest overall effect size ($d = 0.401$), which follows the above results for amplitude characterization, demonstrating that the neural response magnitude is highly responsive to increments in amplitude (see Fig. 3A, left panel). The overall effect size for pulse width is smaller ($d = 0.127$), but still demonstrates an influence on stimulus response magnitude, which follows the results for pulse width characterization where the response magnitude was moderately responsive to increments in pulse width. Lastly, the overall effect size for frequency was negative and minimal ($d = -0.009$), which correlates with its largely insignificant effect on the neural response magnitude (see Fig. 2C) and seemingly suggests that frequency can actually inhibit the magnitude of neural response Fig. 4.

Effect sizes were also grouped by condition tested (i.e., low versus high parameters, low versus middle parameters, and middle versus high parameters), where the effect sizes retained the same pattern (see Fig. 3A, right panel). Amplitude's effect size is larger in all conditions, although its effect size is weaker for the mid—high parameter conditions, possibly due to response saturation. Pulse width's effect size is moderate in the low–high and low—mid parameter conditions, although its effect size becomes much smaller in the mid—high condition. Frequency's effect size is small but still present for the low–high and low—mid conditions, but becomes nearly negligible in the mid—high parameter condition.

There are no interactions present between amplitude and pulse width or amplitude and frequency (see Fig. 3B, all panels and Fig. 3D, all panels). There were interactions observed between pulse width and frequency; the interaction between pulse width and frequency in the low—mid parameters indicates an increase in neural response magnitude when mid-range frequencies are combined with mid-range pulse widths in comparison to other low—mid combinations. A more compelling interaction is observed between pulse width and frequency in the mid—high parameter interaction, where combining mid-range pulse width with a mid-range frequency gives a stronger VEP response than other mid—high combinations. There is no interaction between pulse width and frequency in the low—hi parameter condition. This implies the largest responses are elicited from middle pulse widths and middle frequencies.

Discussion

This study has used coherent holographic imaging to record the dynamics and modulation of vagus-evoked potentials at the cortical surface in vivo.

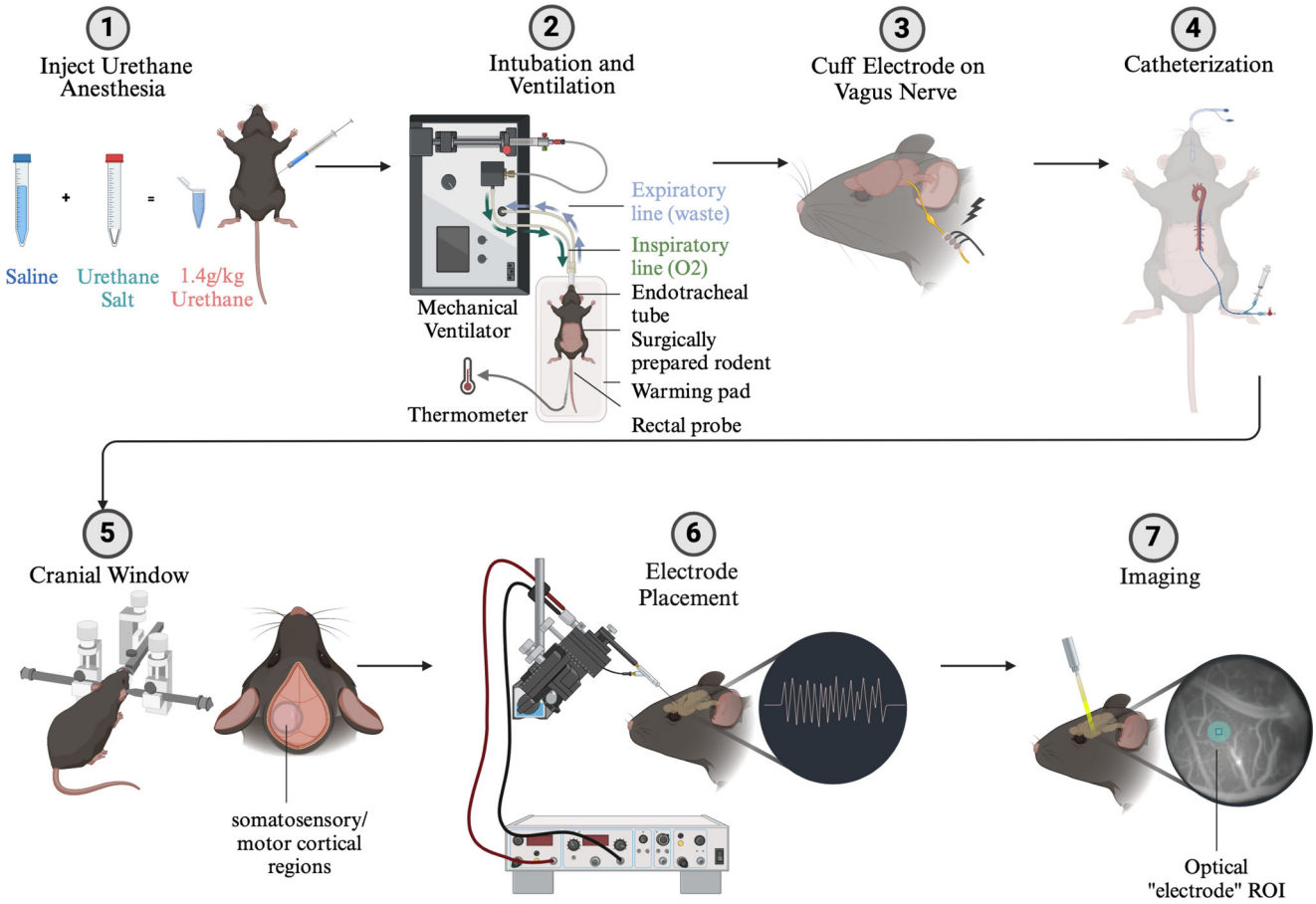

Fig. 4 | Summary of experimental procedures used. (1) Rats were anesthetized with an intraperitoneal injection of urethane. (2) Rats were intubated with an endotracheal tube and mechanically ventilated according to body weight with the Rovent system (Kent Scientific). A homeothermic system maintained body temperature throughout the experiment. (3) A custom-made cuff electrode was surgically implanted around the left vagus nerve. (4) Rats underwent a catheterization of the femoral vein in order to later introduce paralytic agents and fluids. (5) Rats were placed in a stereotaxic frame with a bite bar. A cranial window above the somatosensory and motor cortical regions was made with a dental drill. (6) Silver electrodes were placed over the exposed cortical regions using a micromanipulator (Sensapex). These electrodes were connected to a differential amplifier (AM Systems), and electrical signals were acquired (NI DAQ). (7) The frame was positioned under the beam path of the optical system (denoted by the yellow beam. Color is for visual purposes and does not denote wavelength, which was 1310 nm). Blood vessels were used to change the coherence length of the optical system to bring the surface of the cortex into focus, and an optical region of interest was chosen (teal circle). Figure created with Biorender.com.

The results suggest that changes in stimulus amplitude initiate the greatest modulation of aggregate neural response magnitude, while changes in pulse width drive moderate modulation of neural response magnitude, and changes to stimulation frequency weakly modulate or do not modulate neural response magnitude. These conclusions persisted through parameter randomization at every step to avoid bias and were supported both in isolated characterizations where all other stimulation parameters are held constant and in parameter effect size characterizations where multiple parameter settings were exhaustively combined, each at low, medium, and high magnitudes. These conclusions remain consistent in each of these stimulation contexts across three replicates in each animal. Overall, this study illustrates and quantifies the impact of VNS parameters on cortical response, introduces a non-contact, label-free optical recording method for probing the dynamics and modulation of these responses, and provides a foundation for future investigations into neuromodulation dynamics in other areas innervated by afferent vagal pathways.

Interactions between frequency and pulse width were identified, suggesting that frequencies that are too high or too low may cause response magnitudes to break down. Upon closer inspection of individual responses, it is observed that the lower frequencies tested allowed the tissue velocity to return to a baseline between pulses, while higher frequencies initiated new responses before the previous response returned to baseline. The specific timing (frequency) and duration (pulse width) of this new activation during recovery towards baseline likely have an optimal value that may maximize response magnitude, particularly in animals where long-lasting responses were observed. These observed response timing patterns were consistent within individual animals but widely variable between animals.

Close inspection of the response characteristics demonstrates a delay in cortical activation from stimulus application. This delay in evoked cortical potentials is theorized to arise from synaptic signaling delays, as the initial peripheral stimulation must traverse a polysynaptic pathway through the nucleus tractus solitarius and other possible brainstem nuclei such as the locus coeruleus and dorsal raphe nuclei before reaching cortical targets[22]. As synaptic delays occur in a range of 0.5–1 ms and the vagal afferent pathway is polysynaptic in nature, this serves as a likely explanation for the 5 ms response delay[23].

Notably, there was also a small, repeatable time delay (2–4 ms) between the optical signal and the electrical signal, with the electrical signal preceding, which could arise from several possible sources. One possible source may be attributable to how we measure our optical signal, as we average over a small region of interest (ROI) in the region where the electrode is placed, meaning some distance is incorporated between the optical ROI and the precise location of the electrode. Ultimately, this may create a time delay between them due to the synaptic delays from the signal spatial spread.

Another alternative possibility may be that the electrodes detect these signals faster than the optical system. Electrodes directly capture information about ionic currents and are designed to have nearly instantaneous temporal resolution. While the optical system also has high temporal resolution, it is possible that the detectors for the optical signal, as well as the necessary data processing, may introduce small delays. Light scattering and the intrinsic properties of the tissue may also affect the speed and accuracy of the optical measurements, and these are properties that are harder to control than electrical noise or artifacts. It is also possible that the electrical signal and correlating ionic currents drive the correlating motion measured by the optics, representing a cause-effect sequence visible in these delays. Due to the reasons discussed above, we believe that the presence of a small time delay in the optical signal is reasonable and more intuitive than if the optical signal occurred prior to the electrical signal in time. Additionally, the shape and magnitude of the optical signal and electrical signal are well matched.

Prior studies have suggested that optimizing stimulus parameters can take advantage of the neural circuitry of ascending vagal afferents. One example of this is that the release of norepinephrine by the locus coeruleus is increased by VNS[24,25]; however, while high amplitude and pulse width demonstrably increase the firing rate of the locus coeruleus, modulation of the stimulus frequency does not impact this firing rate[22]. The results of this study suggest that this phenomenon is also present in the cortical response to VNS. While vagus-evoked potentials are modulated by amplitude and pulse width, there is little to no notable modulation by frequency. As VNS changes the availability of norepinephrine in the cortex as a function of locus coeruleus firing activity, this result is perhaps to be expected.

Even in ideal acute stimulation procedures utilizing the same cuff electrode and surgical procedures across several animals, significantly different activation and saturation thresholds were found, ranging from 200 μA to 800 μA, which follows the wide variability observed in other animal studies and human applications. This variability further justifies the need for a rapid-feedback method to individually tune stimulation parameters in each subject, which is made possible on a short time scale with the types of non-contact label-free methods demonstrated here. The findings of this study also serve as a quantitative justification for an updated parameter tuning protocol, utilizing amplitude for coarse adjustments and pulse width for finer adjustments.

The methodology developed in this study—in tandem with the coherent optical system from[26]—to characterize evoked activity on the cortical surface is an advancement in parameter tuning capabilities compared to other functional imaging methods. This is due to the characterization of stimulation parameter effects as well as the non-contact, label-free nature of the optical system. Importantly, this optical modality avoids the presence of stimulus artifact. This is a serious limitation in electrical systems, as the short neural response delays place a limit on the testable pulse widths due to stimulus artifact. There is no other approach known to the authors that can achieve similar spatial and temporal resolution using the non-contact, label-free methodology.

Our digital holographing imaging (DHI) system is advantageous in comparison to other conventional imaging and electrophysiological methods (i.e., EEG, fMRI) in that it does not require labels (dyes, maintenance of transgenic lines, etc...) or contact-dependent methods (electrode insertion, electrode placement). Conventional non-invasive or near non-invasive brain imaging techniques fall into metabolic-based and electrophysiology-based systems. The former are considered to have excellent spatial resolution, but poor temporal resolution, while the opposite is true in the latter. The coherent holography system is a contender for the best of both, as it has a submillisecond temporal resolution and a spatial resolution of 0.1 mm^3 [26]. Its field of view is also over 3 mm in diameter. In comparison to other functional imaging methodologies, this spatiotemporal resolution becomes an apparent advantage. In fMRI, for example, the temporal resolution is limited by the response time of hemodynamics, as the response has a peak that typically occurs 5—6 s after the onset of a neural stimulus. Neural activity tends to be much faster than the hemodynamic response, and, thus, the temporal resolution of this activity is blurred when it is visualized through fMRI[27]. Spatially, fMRI is also limited compared to our optical system, as its voxel size is ~3–4 V with clinical MRI machines[27]; however, in research-specific systems with higher field magnets, MRI can reach voxel sizes of < 0.5 mm[28]. EEG is another commonly used tool to understand functional activity and, like our optical system, has submillisecond temporal resolution[29]; however, its spatial resolution is quite poor, as it is only able to offer a resolution within a range of 5–8 cm at best[30,31]. However, while the coherent optical system may have the advantage spatiotemporally, these conventional systems can be implemented non-invasively and thus offer the greatest current clinical advantage—as this system only offers a step towards more effective non-invasive imaging.

In order to address issues with selection bias in the stimulation parameters, stimulation parameter randomization was implemented rigorously in several stages: Selected parameters were randomized anew in each of the independent trials performed with stimulation, with null trials incorporated into this randomization. Additionally, interstimulation delays were created to ensure the tissue's return to baseline. We further imposed randomized parameters in the parameter combination trials, where we exhaustively combined parameter values and randomized the order in which we stimulated with these combinations. Our observations remained consistent through each randomized parameter application, across at minimum three replicates in each animal, as well as in multiple experimental protocols.

Additionally, analysis for all experimental trials was blinded to the stimulation parameters used in order to avoid confirmation and observer bias while the data was analyzed. All analysis of the signal's identification, maximum displacement and other characteristics was completed without knowledge of which parameters were changing or what the values of these parameters were. To avoid sampling bias, all stimulation parameters and combinations were based on a comprehensive range of stimulation parameters used in several animal studies of VNS, as these parameter ranges represented the general population of parameters available for use in rodent models. We did not attempt to include parameters that posed risks to nerve structure and function, though some of these parameters have been effective in human studies.

While frequency showed little to no effect on cortical activation, this may be limited by the chosen stimulation protocols. Our brief stimulus application never lasted longer than 5 s. This was chosen to contain enough individual responses for sufficient averaging to generate clean repeatable neural responses, while also being brief enough to enable consideration of a wide range of stimulus parameters, parameter combinations, and replicates within a reasonable experimental timeline. However, clinically effective stimulation protocols often last for a minimum of 30 seconds and can be as long as multiple hours or indefinite. Frequency may play a role in affecting circuit dynamics at these longer time scales; however, this was outside the scope of this study.

In initial experiments used for methodology development, we noticed amplitude degradation over time that was attributable to the drying of the exposed dura, leading to increased rigidity and dampening of the response magnitude. We were able to correct this by keeping the cortical window moist, applying frequent irrigation between recordings, and covering the window with moistened hemostatic foam during extended periods between recording sequences. It is critical to keep the cortical window moist and compliant during all recordings, as only when this was true did we see stable response magnitude throughout multiple hours of recordings.

The DHI system measures tissue velocity, which has been shown to correlate with neural activity. The mechanism behind this is still under investigation, and tissue motion accuracy is affected by the vascularization of the neural tissue—which experiences phases of both expansion-contraction and high-low stiffness throughout the cardiac cycle. Noise from vasculature was mitigated here by choosing ROIs which avoided capturing blood vessels to maximize the signal-to-noise ration, preferential weighting of non-cardiac pixels, and also by choosing stimulation periods across multiple cardiac cycles to allow for averaging across multiple stimulus applications and multiple cardiac cycles. Furthermore, VNS itself can impact the cardiac cycle as its efferent projections innervate the heart.

Periodically, it was observed that select frequencies near the heart rate would recruit the heart to fire in sync with stimulation. This caused cardiac artifacts to become stimulus-aligned, persist through averaging, and obscure the averaged neural response. Trials containing this phenomenon were obvious and were excluded from the results; however, this limited the precise frequencies available for characterization in certain animals. Other stimulation side-effects, including hemodynamic effects like blood vessel dilation, have also been observed, and have been cited to occur 1 to 1.5 seconds from stimulation onset[32]. While these are stimulus-locked, they do not occur on a time scale that significantly distorts the shape of the millisecond-resolution response considered in this study.

Confounding motion artifacts can also be introduced by side effects from stimulation, including muscle twitching. While we mitigated this limitation here with verification of our findings in paralyzed animals and in post-mortem trials to remove correlated muscle activity, this motion artifact remains a relevant limitation of the system that must be continuously monitored in all studies utilizing the DHI system.

This paper presents both methodology and analysis tools applied to an accessible, well-established peripheral stimulation model. With this framework, implementation of these same procedures noninvasively is planned. Imaging VNS-evoked responses through skin and skull would provide a clinically translatable, direct feedback measure for VNS patients who will benefit from optimized stimulation parameters. The continued studies of VNS-evoked responses will enable a better understanding and optimization of neural activation from VNS afferent pathways in epilepsy subjects; furthermore, continued study may lead to further insights into the therapeutic mechanism behind VNS in epilepsy.

Correlation between neural activity and the optical response recorded by the system has been confirmed primarily through the use of concurrent electrical recording in our work as well as prior literature[26]; however, work to elucidate the exact relationship between neuronal activity and this evoked optical response is needed. Lefebvre et al., 2023 noted that, following application of penicillin to the cortex to incite synchronous activity, EEG sharp waves could be detected in a range of 75–25 microvolts in amplitude, and these corresponded to optical velocity changes of 500 microns/second[26]. Future experiments expanding this work would likely involve forming direct analogs between the evoked optical response and electrophysiological measures such as firing rate or voltage. Specifically, conducting patch clamp electrophysiology of primary neuronal cultures in tandem with the coherent optical system could form a path toward understanding the evoked optical responses formed by single-cell firing activity.

Future work will also focus on characterizing VEP spatial dynamics and may bring additional insight into the neural activation resulting from VNS—dynamics that may be more difficult to study using other functional imaging modalities due to their lack of sufficient spatiotemporal resolution. The DHI system uniquely offers a wide FOV with sufficiently fine spatial resolution and multi-kilohertz sampling frequencies, all measured using methods that do not contact or interfere with the delicate neural circuitry or application of labels. These specifications are particularly well suited for targeted neuromodulation experiments, where researchers aim to maximize or minimize activation of cortical regions by only adjusting attributes of the applied stimulation. This can incorporate more sophisticated stimulation strategies, including current steering or temporal interference stimulation techniques, which preferentially activate isolated regions of a nerve and its downstream targets. Preliminary data demonstrating spatially independent response dynamics and modulated activation using current steering is shown in the supplementary information (Supplementary Fig. 4), where we attempted to independently control cortical responses of two areas of the cortex. While these preliminary results are encouraging and relevant to justify the potential impact of future work that these results will support, we exclude them from the main text as neuromodulation objectives call for a more focused study design and replicate to reach the statistical standards we have adhered to in our current results.

There is also potential for this technology to be translated to non-invasive imaging of human cortical activity, and some initial feasibility studies are ongoing and seeing early success. When considering the work presented here, while our physical procedures and surgical techniques are far from relevant in humans, the stimulation protocols we have developed could be utilized directly into clinical simulation workflows to support the comprehensive characterization of stimulation parameter effects. If paired with a DHI system that is successful in human applications, this represents a non-invasive cortical feedback tool with stimulation parameter testing protocols that could provide excellent optimization of VEP dynamics, performed with no preparatory steps within the time frame of an extended doctor office visit.

Our work demonstrates the optical system's ability to characterize and image the dynamics of VNS-evoked neural activity in healthy animals; however, in order for this to become clinically relevant further work must understand how these dynamics are altered by seizure states and how VNS treatment paradigms may return this activity to pre-seizure baselines. For these data to be obtained, the optical system must be used to visualize and monitor changes to VNS-evoked potentials in chronic models of epilepsy, such as those induced by kainic acid. Additionally, important will be to visualize how these dynamics change during seizure when VNS seizure-reduction protocols such as those from prior literature are used[5,33–35].

The combination of a novel imaging modality applied to a well-established peripheral stimulation model demonstrated the ability to characterize VNS-evoked neural responses and their dynamics in response to peripherally-driven stimulation. The results show VNS-evoked cortical responses increase as both stimulation current amplitudes and pulse widths increase. The results also demonstrate that frequency has a minimal modulatory effect on these responses. Digital holographic imaging enabled non-contact, label-free characterization and parameter tuning of VNS stimulation, enabling rapid subject-specific parameter tuning. This technology could lead the way toward a non-invasive feedback mechanism and targeting strategies that may increase the efficacy of VNS in all patients with refractory epilepsy.

Methods

Optical

Previous studies have found evidence of optical property fluctuations in neural tissue in vitro that are well-correlated to concomitant neural activation[36–39]. These optical changes have become of high interest, as these signals represent a feasible functional imaging approach to capturing aggregate neural responses without the need for structural or functional tags, such as those in calcium imaging or fluorescence spectroscopy.

To record functional imaging correlates of VNS, we make use of a phase-driven coherent optical system called "digital holographic imaging" developed by the Applied Physics Laboratory, to detect population-level neuronal responses for use in vivo[26]. DHI is a label-free functional imaging technique that uses holography to measure nanometer-scale tissue displacements with high spatiotemporal accuracy.

Following the works presented by Lefebvre[26], our optical imaging system uses an interferometer to illuminate the exposed cortical surface with a coherent laser source (SLD1018P, ThorLabs) at skin-safe power. A superluminescent diode source (SLD1018P, Thorlabs) with a center wavelength of 1310 nm was split between an object beam and a reference beam by a beam splitter. The collimated object beam illuminated the sample plane at ~96 mW. The light that scattered off of the neural tissue from this collimated beam was collected and mixed with light from the reference beam, forming a hologram. Complex image information from this hologram was then gathered and reconstructed using a Fresnel transform. Processing of this complex image was performed using custom MATLAB software[26]. The phase information in these complex images is used to track phase changes from optical scatterers within the tissue to calculate the velocity of neuronal tissue displacement. This velocity profile serves as the basis for measuring aggregate cortical activation. Imaging frames recorded a roughly 4 mm-diameter area of tissue at a 64×64 resolution at 4 kHz, and were triggered using custom MATLAB and Python software[26]. Holograms were acquired with a CRED3 camera (First Light Imaging, Axion Optics).

In each animal, the imaging system was roughly focused on a section of cortical surface near the primary somatosensory cortex with minimal vasculature, as this area has been shown to be activated in VNS paradigms[32]. Rats were positioned and imaged on a floating table to limit artifacts from movement. After progressively increasing stimulation amplitude to observe a clear neural response, the region of interest was imaged at several depths separated by 1 mm. The depth at which the largest response occurred was selected as the principal region of interest. The largest response was typically noted at around 1–2 mm below the surface of the dura.

Electrical

Twisted pair electrode. Twisted pair electrodes were prepared by depositing 3–4 μm of parylene on two 0.25 mm-diameter silver wires and twisting together. The ends of one end were cut to expose the wire tips to the recording site, and the other ends stripped and connected to an AM Systems Differential AC Amplifier (Model 1700) configured with between 60 dB and 80 dB of gain and a bandpass filter from 10 Hz to 10 kHz.

Cuff electrode. A custom-made cuff electrode was made by sewing 75 μm Platinum Iridium wire into a silicone tube (AM Systems, catalog #806700), creating two rows of electrical contacts on the inner surface each measuring 1 mm long and separated by a 1 mm gap. The cuff's outer surface was insulated with a teflon coating on the wire and an additional medical-grade silicone layer.

Stimulator circuitry. A mirrored Howland current source, as described in ref. 40, was used with the addition of larger DC blocking capacitors (labeled C2) to enable biphasic square wave stimulation. With the cathode proximal, bursts of 50 negative-positive pulse pairs were applied, cathode-first, with 200 μs between pulses. At least 35 seconds were reserved after each pulse burst to allow for the tissue's return to baseline. Orofascial or neck-related musculature twitching (which can occur as off-target effects of VNS) was not observed in any of the rats included in this study. All control waveforms were generated using an NI USB-6353 DAQ at 250 kHz and custom-made scripts in MATLAB and Python.

Surgical

Female ($N = 7274 \pm 39$ g; range 218–308 g; Envigo) and male ($N = 10{,}287 \pm 27$ g; range 237–324 g; Envigo) Long Evans rats were anesthetized with an intraperitoneal injection of urethane (1.4 g/kg). A thermostatically-controlled heating pad maintained core body temperature at 37 °C throughout the course of the experiment.

All surgical procedures were approved by the Johns Hopkins University Animal Care and Use Committee. Data from a total of 17 animals is presented, and an additional 22 animals were used in methodology development for this study. Animals were housed in same-sex pairs under a 12:12: light–dark cycle, with ad libitum access to food and water. Additional animal information can be found in the supplementary information (Supplementary Table 1).

Cuff electrode implantation. A sagittal incision of ~3 cm in length was made on the ventral aspect of the neck. The submaxillary gland and connective tissue were retracted. The left sternomastoid and omohyoid muscles were bluntly dissected and separated until the left vagus nerve was revealed. The left vagus nerve was characterized as lying lateral to the carotid artery and was isolated from the artery and the remaining vessels in the carotid sheath. Once isolated, the nerve was sleeved into the lumen of the cuff electrode. The cuff electrode was then sutured around its circumference to secure the nerve inside and ensure appropriate electrode contact. The leads from the electrode were drawn between the subcutaneous fascia and musculature to the initial incision, which was then sutured around the leads to secure them. Following the end of imaging and recording, euthanasia (sodium pentobarbitol with phenytoin) was administered intraperitoneally.

Venous catheterization. The femoral vein of some study animals was cannulated in order to administer rocuronium paralytic. An incision of approximately 15 mm was made in the inguinal area, and a blunt dissection of the connective tissue was performed until the femoral vein and artery were revealed. The catheter was connected to a three-way stopcock, which was connected to two syringes containing heparizined saline (20 U/mL) and rocuronium (10 mg/mL), respectively. Using microdissection scissors, a small cut in the vein was made at a 45-degree angle, taking care not to cut through the vein. Fine tipped forceps were fed into the incision and opened, allowing for the placement of the catheter into the vein. The catheter was fully inserted, after which all knots were tightened, and the last silk piece was knotted around the venal tissue holding the catheter.

Cranial window. Rats were then moved into a stereotaxic frame. The scalp skin and subcutaneous fascia were resected to reveal the whole dorsal area of the skull. The periosteum was removed, and a circular craniotomy with a diameter of 5 mm was made using a dental drill over an area encompassing a large region of the sensorimotor cortex. The dura was kept intact for all surgeries and sterile lactated ringer's solution irrigation was used to maintain moisture throughout the duration of the experiments. The moistened hemostatic foam was also used during extended periods between imaging to reduce bleeding and maintain hydration.

Paralytic and ventilation. In a subset of experiments ($N = 8$), some rats were paralyzed with intravenous administration of rocuronium (1 mg/kg). An endotracheal tube was used to intubate the animal, and the Rovent system (Kent Scientific) was used to mechanically ventilate the animal for the duration of the experiment. Rocuronium was applied through the venous catheter with an initial bolus of 5 mg/mL and updates of 1 mg/mL every 25 minutes. Mechanical ventilation was stopped for up to 10 seconds during optical recording to reduce motion.

Experimental

Electrical validation. In a subset of experiments, optical and electrical signals were simultaneously recorded for the purpose of validating the presence and dynamics of the optical signal. The tips of the twisted pair electrode were positioned to lightly rest on the surface of the dura within the optical recording FOV. Stimulus was applied at increasing amplitudes until a stimulus-locked response was observed in both electrical and optical recordings. Low, medium, and high stimulus currents were applied to verify coordinated response changes in both recordings. Shorter pulse widths (≤ 200 μs) were required in these experiment trials to avoid contaminating the electrical response with stimulus artifact, as only at these shorter pulse widths was the stimulation artifact clearly separable from the dose-dependent response also seen in the optical signal. Notably, the optical response does not have this limitation as it is not impacted by electrical stimulus artifact.

Amplitude characterization. First, a minimum current amplitude at which no cortical response could be recorded was found. A maximum current amplitude at which the cortical response reached a maximum value, and saturated was also found. Within this range, a sequence of trials with randomized current amplitudes was delivered at constant pulse width (500 μs) and frequency (13 or 15 Hz to avoid heart rate coupling), with 50 pulses per trial and at least 35s between trials. A null trial (0 μA) was randomly placed in each sequence. This sequence of amplitude sweeps was repeated for a total of three sweeps throughout the course of the experiment.

At the end of the experiments following the injection of the euthanasia compound, the cessation of diaphragmatic deflection was monitored, and an additional amplitude characterization was performed for control purposes. Additionally, to control for motion artifact in a population of animals $N = 8$, a paralytic was administered throughout the stages of

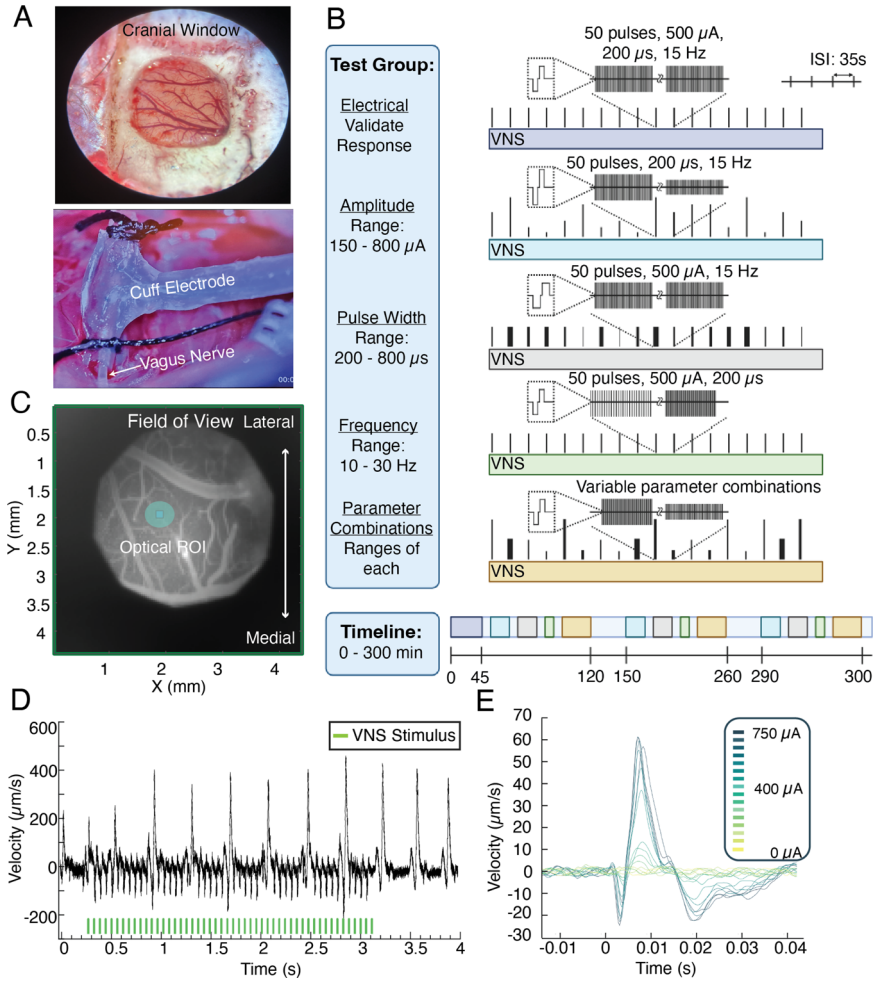

Fig. 5 | Summary of imaging and stimulation procedures. A Top—representative image of a Cranial Window with vasculature. Bottom—cuff electrode around the left vagus nerve. **B** Visualization of stimulation protocol. Five sequence types were used to consider electrical validation, amplitude response, pulse width response, frequency response, and randomized combinations of parameters. Experiments consisted of iterations of these sequences across ~300 min. **C** Hologram magnitude image showing the imaged tissue. This allows the selection of ROI coordinates (teal circle), which avoids large vasculature. **D** Velocity data from a selected ROI. 50 stimulus pulses are applied (green bars), and in this trial, responses can be seen after each individual stimulus pulse. **E** Overlayed responses from an amplitude sequence. Each individual trace represents the response after temporal alignment and averaging of all 50 pulses applied at that parameter setting. **B** created using Biorender.com.

experimentation. In tandem with mechanical ventilation, the responses recorded here served not only as verification that the responses were not attributable to motion, but also as a control for the responses recorded without auxiliary ventilation.

Pulse width characterization. After at least one amplitude characterization, an amplitude just above the threshold and below saturation was chosen. A minimum pulse width at which no cortical response could be recorded was found, and a maximum pulse width duration at which the cortical response reached a maximal magnitude and experienced saturation was also found. Within this range, a sequence of trials with randomized pulse widths was performed at a constant amplitude and frequency, with 50 pulses per trial and at least 35 s between trials. A null trial (amplitude of 0 μA) was randomly placed in each trial sequence. This sequence of pulse width sweeps was repeated for a total of three sweeps throughout the course of the experiment.

Frequency characterization. To determine vagus-evoked potential modulation as a function of stimulus frequency, a nominal literature-based range of typical frequencies utilized in VNS[11] was created from 10 Hz to 30 Hz. Frequencies above 30 Hz were not used to avoid damaging the nerve. This range of frequencies was then used for stimulation. The stimulation was delivered in blocked trials, with 50 pulses per trial and at least 35 s between trials. A null trial (amplitude of 0 μA) was randomly placed in each trial sequence.

Effect size characterization. After at least one sweep of each amplitude, pulse width, and frequency characterization, a combinatorial protocol was chosen to delineate the effect sizes for each parameter. In this paradigm, low, medium, and high values for each parameter were selected. These values were then used to create an array of randomized combinations to test for the effect sizes of each parameter as well as interactions between the low and high values, low and medium values, as well as medium and high values. This entire sequence of stimulus combinations was delivered in blocked trials, with 50 pulses per trial and at least 35 s between trials. The whole trial sequence was randomized and repeated three times over the course of the experiment, with at least 30 minutes between each sequence. A null trial with a stimulus amplitude of 0 μA was randomly placed within each sequence.

Data processing

Optical. The imaging data were processed using the methodology described in ref. 26, generating velocity measurements for the entire FOV over time, which correlated to the neural responses. To analyze response characteristics and effect sizes, a single ROI of a diameter of 0.4 mm was selected in a tissue area with minimal vasculature—specifically where maximal signal-to-noise ratio was observed (see Fig. 5C). All velocity data within this ROI was averaged to mitigate phase noise from the optical system. For each trial, the individual responses to each of the 50 stimulus pulse pairs were temporally aligned and averaged, defining the evoked response. The response magnitude was characterized by the initial stimulus-aligned upward deflection in tissue velocity (see Fig. 5E), which consistently occurred around 5 ms ± 1 ms post-stimulation. The minimum and maximum velocities along this deflection were annotated, and the difference between these points defined the response magnitude for a given trial. Any VNS-evoked response that did not have a deflection

greater in magnitude than spontaneous or baseline activity was discarded.

Experimental. Comparisons across animals for the stimulus response characteristics and parameter sensitivity analyses were achieved by normalizing all response magnitudes to the maximum signal magnitude observed in a particular animal. The stimulus parameters being tested were also normalized to the maximum value of the range tested stimuli. A description of the range of parameters applied can be found in the supplementary information (Supplementary Table 1).

Statistical analyses. Data were examined for normality (Shapiro–Wilk). Non-parametric results from amplitude, pulse width, and frequency characterizations were presented as means ± standard error of the mean and analyzed using Welch's two-tailed *t* test. Effect size results were presented as standard deviations of the mean and calculated using Cohen's *D* assessment. A calculated p value of <0.05 was considered significantly different.

Effect size and interaction. The parameter effect size, or the value of Cohen's *D*, was determined by calculating the average normalized response for two parameter settings (e.g., for factor A low–high effect size, the normalized velocity response for the low amplitude setting and high amplitude settings were found separately, each including all other settings of all other parameters) and taking the difference between the means, then dividing by the standard deviation of the condition's dataset (i.e., low–high). ($N = 8$ animals). The parameter comparisons were as follows: "low–high" stimulus parameters, "middle—high" stimulus parameters, and "low—middle" stimulus parameters. Interaction plots were then created for each parameter comparison to visualize the interactions of stimulus factors, where parallel lines indicate no interaction and intersecting lines signify some interaction. Interaction plots were calculated by finding the average normalized evoked response for a condition-specific combination of parameters (i.e., A LO, A HI against P-LO, P-HI) and plotting these against each other to understand whether particular combinations of parameters could optimize the magnitude of the evoked signal. Each interaction plot displayed the levels of one condition on the horizontal axis and had a separate plotted line for each level of the other condition. Amplitude is represented as factor "A" or "Amp", pulse width is represented as factor "P" or "Pulse", and frequency is represented as factor "F" or "Freq".

Received: 19 April 2024; Accepted: 17 August 2024;
Published online: 10 September 2024

References

1. Fisher, R. S. et al. ILAE official report: a practical clinical definition of epilepsy. *Epilepsia* **55**, 475–482 (2014).
2. Fiest, K. M. et al. Prevalence and incidence of epilepsy. *Neurology* **88**, 296–303 (2017).
3. French, J. A. Refractory epilepsy: clinical overview. *Epilepsia* **48**, 3–7 (2007).
4. Howland, R. H. Vagus nerve stimulation. *Curr. Behav. Neurosci. Rep.* **1**, 64–73 (2014).
5. Zabara, J. Inhibition of experimental seizures in canines by repetitive vagal stimulation. *Epilepsia* **33**, 1005–1012 (1992).
6. Ben-Menachem, E. et al. Vagus nerve stimulation for treatment of partial seizures: 1. a controlled study of effect on seizures. *Epilepsia* **35**, 616–626 (1994).
7. Rush, A. J. et al. Vagus nerve stimulation (VNS) for treatment-resistant depressions: a multicenter study. *Biol. Psychiatry* **47**, 276–286 (2000).
8. Sackeim, H. A. et al. Vagus nerve stimulation (VNS) for treatment-resistant depression: efficacy, side effects, and predictors of outcome. *Neuropsychopharmacology* **25**, 713–728 (2001).
9. Lomarev, M. et al. Vagus nerve stimulation (VNS) synchronized BOLD fMRI suggests that VNS in depressed adults has frequency/dose dependent effects. *J. Psychiatr. Res.* **36**, 219–227 (2002).
10. Musselman, E. D., Pelot, N. A. & Grill, W. M. Empirically based guidelines for selecting vagus nerve stimulation parameters in epilepsy and heart failure. *Cold Spring Harb. Perspect. Med.* **9**, a034264 (2019).
11. Thompson, S. L. et al. A review of parameter settings for invasive and non-invasive vagus nerve stimulation (VNS) applied in neurological and psychiatric disorders. *Front. Neurosci.* **15**, 709436 (2021).
12. Wheless, J. W., Gienapp, A. J. & Ryvlin, P. Vagus nerve stimulation (VNS) therapy update. *Epilepsy Behav.* **88**, 2–10 (2018).
13. Schuerman, W. L. et al. Human intracranial recordings reveal distinct cortical activity patterns during invasive and non-invasive vagus nerve stimulation. *Sci. Rep.* **11**, 22780 (2021).
14. Kibleur, A. et al. Electroencephalographic correlates of low-frequency vagus nerve stimulation therapy for Crohn's disease. *Clin. Neurophysiol.* **129**, 1041–1046 (2018).
15. Hammond, E. J., Uthman, B. M., Reid, S. A. & Wilder, B. J. Electrophysiological studies of cervical vagus nerve stimulation in humans: I. EEG effects. *Epilepsia* **33**, 1013–1020 (1992).
16. Salinsky, M. C. & Burchiel, K. J. Vagus nerve stimulation has no effect on awake EEG rhythms in humans. *Epilepsia* **34**, 299–304 (1993).
17. Yakunina, N., Kim, S. S. & Nam, E.-C. Optimization of transcutaneous vagus nerve stimulation using functional MRI. *Neuromodulation* **20**, 290–300 (2017).
18. Ernst, L. D. et al. Electrocorticography analysis in patients with dual neurostimulators supports desynchronization as a mechanism of action for acute vagal nerve stimulator stimulation. *J. Clin. Neurophysiol.* **40**, 37–44 (2023).
19. Yokoyama, R. et al. The immediate effects of vagus nerve stimulation in intractable epilepsy: an intra-operative electrocorticographic analysis. *Neurol. Med. Chir.* **60**, 244–251 (2020).
20. Zhang, J., Xia, J. & Xiong, H. Techniques for extracellular recordings. *In:* Xiong, H. & Gendelman, H. E. (eds.) *Current Laboratory Methods in Neuroscience Research*, 325–345 https://doi.org/10.1007/978-1-4614-8794-4_23 (Springer, New York, NY, 2014).
21. Koponen, L. M. et al. Transcranial magnetic stimulation input-output curve slope differences suggest variation in recruitment across muscle representations in primary motor cortex. *Front. Hum. Neurosci.* **18**, 1310320 (2024).
22. Hulsey, D. R., Shedd, C. M., Sarker, S. F., Kilgard, M. P. & Hays, S. A. Norepinephrine and serotonin are required for vagus nerve stimulation directed cortical plasticity. *Exp. Neurol.* **320**, 112975 (2019).
23. Caire, M. J., Reddy, V. & Varacallo, M. Physiology, snapse. In: *StatPearls* (StatPearls Publishing, Treasure Island (FL)). http://www.ncbi.nlm.nih.gov/books/NBK526047/ (2024).
24. Manta, S., Dong, J., Debonnel, G. & Blier, P. Enhancement of the function of rat serotonin and norepinephrine neurons by sustained vagus nerve stimulation. *J. Psychiatry Neurosci.* **34**, 272–280 (2009).
25. Roosevelt, R. W., Smith, D. C., Clough, R. W., Jensen, R. A. & Browning, R. A. Increased extracellular concentrations of norepinephrine in cortex and hippocampus following vagus nerve stimulation in the rat. *Brain Res.* **1119**, 124–132 (2006).
26. Lefebvre, A. T. et al. High-resolution label-free transcranial imaging of in vivo neural activity via interferometric measurement of tissue deformation. https://www.biorxiv.org/content/10.1101/2023.10.05.561052v1.full (2023).
27. Glover, G. H. Overview of functional magnetic resonance imaging. *Neurosurg. Clin. North Am.* **22**, 133–139 (2011).
28. Shmuel, A., Yacoub, E., Chaimow, D., Logothetis, N. K. & Ugurbil, K. Spatio-temporal point-spread function of fMRI signal in human gray matter at 7 Tesla. *NeuroImage* **35**, 539–552 (2007).

29. Burle, B. et al. Spatial and temporal resolutions of EEG: is it really black and white? A scalp current density view. *Int. J. Psychophysiol.* **97**, 210–220 (2015).
30. Nunez, P. L. et al. A theoretical and experimental study of high resolution EEG based on surface Laplacians and cortical imaging. *Electroencephalogr. Clin. Neurophysiol.* **90**, 40–57 (1994).
31. Ferree, T. C., Clay, M. T. & Tucker, D. M. The spatial resolution of scalp EEG. *Neurocomputing* **38-40**, 1209–1216 (2001).
32. Collins, L., Boddington, L., Steffan, P. J. & McCormick, D. Vagus nerve stimulation induces widespread cortical and behavioral activation. *Curr. Biol.: CB* **31**, 2088–2098.e3 (2021).
33. Krahl, S. E. Vagus nerve stimulation for epilepsy: a review of the peripheral mechanisms. *Surg. Neurol. Int.* **3**, S47–S52 (2012).
34. Katagiri, M. et al. Anti-seizure effect and neuronal activity change in the genetic-epileptic model rat with acute and chronic vagus nerve stimulation. *Epilepsy Res.* **155**, 106159 (2019).
35. Takaya, M., Terry, W. J. & Naritoku, D. K. Vagus nerve stimulation induces a sustained anticonvulsant effect. *Epilepsia* **37**, 1111–1116 (1996).
36. Lee, H. J., Jiang, Y. & Cheng, J.-X. Label-free optical imaging of membrane potential. *Curr. Opin. Biomed. Eng.* **12**, 118–125 (2019).
37. Ling, T. et al. High-speed interferometric imaging reveals dynamics of neuronal deformation during the action potential. *Proc. Natl. Acad. Sci.* **117**, 10278–10285 (2020).
38. Batabyal, S. et al. Label-free optical detection of action potential in mammalian neurons. *Biomed. Opt. Express* **8**, 3700–3713 (2017).
39. Akkin, T., Landowne, D. & Sivaprakasam, A. Detection of neural action potentials using optical coherence tomography: intensity and phase measurements with and without dyes. *Front. Neuroenerget.* **2**, 22 (2010).
40. Budde, R. B., Williams, M. T. & Irazoqui, P. P. Temporal interference current stimulation in peripheral nerves is not driven by envelope extraction. *J. Neural Eng.* **20**, 026041 (2023).

Acknowledgements

We specifically thank the Applied Physics Lab for their diligent work in developing this imaging system and the holography processing paradigm, which enabled our use of it with VNS in this study. This work was funded by NIH NS119390.

Author contributions

L.R.: conceptualization of this study, methodology, surgery, analysis, writing. T.M.: conceptualization of this study, methodology, software, analysis, writing. T.P.: methodology, analysis. P.I.: advisor, conceptualization of this study.

Competing interests

The authors declare no competing interests.

Additional information

Supplementary information The online version contains supplementary material available at https://doi.org/10.1038/s44328-024-00012-z.

Correspondence and requests for materials should be addressed to Laura RoaFiore.